THE JOURNAL OF BIOLOGICAL CHEMISTRY
Vol. 280, No. 22, Issue of June 3, pp. 21246–21255, 2005
Printed in U.S.A.

Identification of a Novel Pharmacophore for Peptide Toxins Interacting with K^+ Channels*

Received for publication, March 3, 2005, and in revised form, March 29, 2005
Published, JBC Papers in Press, March 30, 2005, DOI 10.1074/jbc.M502376200

Laurent Verdier‡§, Ahmed Al-Sabi¶, Jean E. F. Rivier‖, Baldomero M. Olivera, Heinrich Terlau¶‡‡, and Teresa Carlomagno‡§§§**

*From the ‡Department of NMR-based Structural Biology, Max Planck Institute for Biophysical Chemistry, Am Fassberg 11, D-37077 Göttingen, Germany, ¶Group of Molecular and Cellular Neuropharmacology, Max Planck Institute for Experimental Medicine, Hermann-Rein-Strasse 3, D-37075 Göttingen, Germany, ‖The Clayton Foundation Laboratories for Peptide Biology, The Salk Institute, La Jolla, California 92037, and **Department of Biology, University of Utah, Salt Lake City, Utah 84112*

κM-conotoxin RIIIK blocks TSha1 K^+ channels from trout with high affinity by interacting with the ion channel pore. As opposed to many other peptides targeting K^+ channels, κM-RIIIK does not possess a functional dyad. In this study we combine thermodynamic mutant cycle analysis and docking calculations to derive the binding mode of κM-conotoxin RIIIK to the *TSha1* channel. The final model reveals a novel pharmacophore, where no positively charged side chain occludes the channel pore. Instead the positive-charged residues of the toxin form a basic ring; κM-RIIIK is anchored to the K^+ channel via electrostatic interactions of this basic ring with the loop and pore helix residues of the channel. The channel amino acid Glu-354 is likely to be a fundamental determinant of the selectivity of κM-RIIIK for the *TSha1* channel. The Cγ-OH of Hyp-15 is in contact with the carbonyls of the selectivity filter, disturbing the charge distribution pattern necessary for the coordination of K^+ ions. This novel, experimentally based pharmacophore model proves the existence of diverse binding modes of peptidic toxins to K^+ channels and underlines the role of intermolecular electrostatic interactions involving channel loop side chains in determining the selectivity of toxins for specific K^+ channel types.

Potassium (K^+) channels are a very diverse group of proteins that are key elements for a variety of different physiological functions including the electrical excitability of cells (1). During evolution a great variability of peptide toxins targeting different K^+ channels have been evolved by several venomous organisms including snakes, spiders, and scorpions. The venoms of the marine cone snails are known to contain different families of peptides, the so-called conotoxins, which target ligand-gated and voltage-gated ion channels with great specificity. Meanwhile several conotoxins have been identified that have been shown to interact with voltage-activated K^+ channels. This includes the κ-conotoxins and the κM-conotoxins (2).

Recently the structure of κM-conotoxin RIIIK (κM-RIIIK),[1] a peptide obtained from a venom duct library from *Conus radiatus*, was solved by NMR analysis (3). κM-RIIIK is known to block *Shaker* and mammalian Kv1.2 K^+ channels, whereas the highest affinity target so far identified is *TSha1*, a *Shaker*-related K^+ channel from trout (4, 5). Despite the entirely different pharmacological specificity, a high structural similarity has been observed between this peptide and μ-conotoxin GIIIA, which specifically blocks Na^+ channels, or ψ-conotoxin PIIIE, which is a non-competitive blocker of nicotinic acetylcholine receptors.

Structurally and phylogenetically unrelated toxins that interact with voltage-activated K^+ channels usually share a dyad motif composed of a lysine and a hydrophobic amino acid residue (Tyr or Phe). In particular, there is evidence that the lysine residue of this functional dyad occludes the K^+ channel pore (6–8). This dyad has been proposed to be the minimal core domain of the K^+ channel binding pharmacophore (9–12). A systematic mutational analysis conducted for all non-cysteine residues of κM-RIIIK showed that κM-RIIIK does not contain a functional dyad (3), in contrast to most K^+ channel-targeting peptidic neurotoxins. In κM-RIIIK all the residues that are most relevant for function contain a positive charge; these residues define a basic ring separating two peptide surfaces. The peptide residues that are moderately relevant for binding cluster on one of the two surfaces, whereas those that are irrelevant for binding occupy the other surface. Based on the lack of the dyad and on the observation that all the functionally relevant residues are clustered on one surface of the peptide delimited by a ring of positive charges, a novel pharmacophore model was hypothesized for the κM-RIIIK-*TSha1* complex. In this model the ring of positive charges is used as an anchor to residues of the K^+ channel loops, and κM-RIIIK blocks the channel by covering the pore as a lid (3). Additionally, no positively charged side chain penetrates the channel pore. The importance of a ring of basic residues for potassium channel binding was also proposed for the scorpion toxin Pi1 by Mouhat *et al.* (13), indicating that a similar pharmacophore might have independently evolved for cone snails and scorpions.

In this study we investigate the interaction of κM-RIIIK with the pore of the *TSha1* K^+ channel. We use the data from an extensive mutant cycle analysis to calculate the orientation of the peptide within the pore of the *TSha1* channel, whose structure was derived by homology to the known KcsA structure (14). Previous work (7, 15) has demonstrated the validity of a

* This work was financed by Max Planck Gesellschaft and by the BioFuture Prize of the German Ministry of Education and Research (Förderkennzeichen Grant 0311859) (to H. T.). The costs of publication of this article were defrayed in part by the payment of page charges. This article must therefore be hereby marked "*advertisement*" in accordance with 18 U.S.C. Section 1734 solely to indicate this fact.

§ Supported by a fellowship from The Humboldt Foundation.

‡‡ To whom correspondence may be addressed. Tel.: 49-551-389-9474; Fax: 49-551-389-9475; E-mail: hterlau@gwdg.de.

§§ To whom correspondence may be addressed. Tel.: 49-551-201-2214; Fax: 49-551-201-2202; E-mail: taco@nmr.mpibpc.mpg.de.

[1] The abbreviations used are: κM-RIIIK, κM-conotoxin RIIIK; WT, wild type; r.s.m.d., root mean square deviation; O, Hyp.

computational approach based on intermolecular distance restraints, which can be derived by mutant cycle data, for obtaining models of the atomic interactions in bimolecular complexes. In this study the solution structure of κM-RIIIK is docked to the *TSha1* channel, allowing full flexibility of the side chains of both the peptide and the protein and using 17 intermolecular distance restraints derived from experimental mutant cycle data. The resulting model for the κM-RIIIK-*TSha1* complex indicates that κM-RIIIK indeed occludes the permeation pathway as a lid, which is anchored by the electrostatic interaction of a ring of basic residues on the peptide surface with the outer vestibule of the ion channel pore. All functionally relevant residues belong to the interaction surface with the channel, whereas functionally irrelevant side chains are mostly projected toward solution. Specific electrostatic interactions between the positively charged side chains of the toxin and channel residues of the loop and outer helix regions are likely to be responsible for the selectivity of κM-RIIIK for the *TSha1* channel. Furthermore, our model suggests that the *trans*-hydroxyproline 15 of κM-RIIIK, which is the homologous residue of Arg-13 of μ-conotoxins GIIIA, interacts with the carbonyl groups within the selectivity filter of the channel, thereby occupying the permeation pathway. Arg-13 of μ-conotoxins has been demonstrated to be essential for blocking the pore of Na^+ channels (2, 16, 17). Our finding indicates that pharmacologically diverse but structurally similar peptides might interact with their specific targets in a analogous way despite the large differences in the amino acids sequence.

MATERIALS AND METHODS

Molecular Biology—The original DNA clone of the *Shaker*-related K^+ channel (*TSha1*) from the central nervous system of rainbow trout (*Onchorychus mykiss*) was kindly provided by Prof. Dr. G. Jeserich, University of Osnabrück, Germany. *In vitro* site-directed mutagenesis of *TSha1* was performed following standard procedures (18, 19) and according to manufacturer protocols when commercial kits were used. The vector used throughout this study was pSGEM (3118 bp), a modified version of pGEMHE, which was a generous gift of Prof. Dr. Michael Hollmann (Bochum University, Bochum, Germany).

Electrophysiological Recordings and Data Analysis—The two-electrode voltage clamp technique in the *Xenopus* oocyte heterologous expression system was used to investigate the affinities of the toxin mutants for the different channel mutants. Oocyte injection and maintenance was performed as already described (20). The WT and mutant analogs of κM-RIIIK were synthesized, folded, and tested as already described (3, 4). The IC_{50} values for the block of *TSha1* channels were calculated from the peak currents at a test potential of 0 mV according to $IC_{50} = fc/(1 - fc) \times [Tx]$, where *fc* is the fractional current, and [*Tx*] is the toxin concentration. Data are given as the mean ± S.D. The calculation of the interaction free energy ($\Delta\Delta G$) from the electrophysiological data were performed as described earlier (20).

Docking Calculations—The model of the *TSha1* channel was obtained by homology to the crystal structure of the KcsA channel (14) with a procedure similar to that described by Eriksson and Roux (7) to obtain the *Shaker* channel model. A large number of spatial restraints, extracted from the KcsA PDB file (1BL8), were optimized using the program MODELLER Version 6.2 to generate similarity-based models of *TSha1* (21). The ideal 4-fold symmetry of the tetrameric channel was imposed on all the models. Of the 100 generated models, the one with the lowest MODELLER restraint energy was kept and refined by energy minimization with the program CNS solve 1.1 (22) using the "proteinallhdg" forcefield.

The docking protocol was based on a similar procedure as that used by Eriksson and Roux (7). 875 docking models of the complex between the *TSha1* channel model structure and the NMR structure of κM-conotoxin RIIIK were generated with the program CNS solve 1.1 (22) and using mutant cycle derived intermolecular distance restraints. In the thermodynamic double mutant cycle analysis, two interacting molecules A and B are mutated at specific sites *a* and *b* to give two molecules A* and B*. The binding free energies ΔG for the wild type and single and double mutant complexes A-B, A*-B, A-B*, and A*-B* are combined to obtain the interaction free energy, $\Delta\Delta G_{int} = [\Delta G(\text{A*-B*}) - \Delta G(\text{A*-B})] - [\Delta G(\text{A-B*}) - \Delta G(\text{A-B})]$. The $\Delta\Delta G_{int}$ is a measure of the non-additivity of the mutations *a** on A and *b** on B and reveals a direct interaction of the sites *a* and *b* (23, 24). In these studies the $\Delta\Delta G$ values of Fig. 3 were translated into intermolecular distances as follows: (*a*) 2 kJ/mol $< \Delta\Delta G \leq$ 3 kJ/mol corresponds to a very weak intermolecular distance (d) restraint between sites *a* and *b* (4 Å $<$ d $<$ 6 Å); (*b*) 3 kJ/mol $< \Delta\Delta G \leq$ 4 kJ/mol corresponds to a weak intermolecular distance restraint (3.5 Å $<$ d $<$ 5.5 Å); (*c*) 4 kJ/mol $< \Delta\Delta G \leq$ 5.5 kJ/mol corresponds to a medium distance restraint (2.5 Å $<$ d $<$ 4.5 Å); $\Delta\Delta G >$ 5.5 kJ/mol corresponds to a strong distance restraint (1.5 Å $<$ d $<$ 3.5 Å). If *a* and *b* are polar or charged residues, the minimum distance between the heavy atoms of the polar or charged groups has to fulfill the intermolecular distance restraint; for non-polar residue pairs the minimum distance between all heavy atoms of the side chains is used. Because of the 4-fold symmetry of the *TSha1* channel we used ambiguous distance restraints; the distance d_{ij} between a residue of the toxin (*i*) and a residue of the channel (*j*) is described as, $d_{ij} = \text{Min}(\|r_i - r_j^{\text{A}}\|, \|r_i - r_j^{\text{B}}\|, \|r_i - r_j^{\text{C}}\|, \|r_i - r_j^{\text{D}}\|)$, where A, B, C, and D are the four identical subunits of *TSha1*.

To avoid redundant identical complexes, all distances from the residue Arg-10 of κM-RIIIK were assigned to the subunit A of the channel. The NMR structure of κM-conotoxin RIIIK shows that Arg-10 and Lys-18 are on opposite sides of the peptide; to ensure that the toxin is stretched over the pore, we impose that Lys-18 is close to the extracellular loop of the channel unit opposite to that in contact with Arg-10 (unit C). A total of 16 distance restraints were used: three very weak (Val-376–Leu-1, Met-375–Hyp-15, Glu-348–Arg-19), three weak (Glu-348–Leu-1, Met-375–Leu-1, Glu-348–Arg-10, five medium (Glu-354–Leu-1, Pro-349–Leu-1, Glu-348–Lys-18, Glu-354–Arg-19, Ser-351–Arg-19), and five strong (Glu-354–Arg-10, Pro-349–Arg-10, Ser-351–Arg-10, Glu-354–Lys-18, Pro-349–Arg-19). An additional distance restraint was added between the N terminus NH_3^+ of the toxin and any electronic acceptor of the channel, following the dramatic decrease in the toxin affinity upon acetylation of the terminal amine (3). All distances were restrained with a harmonic potential.

The docking protocol consisted of a series of short torsion angle Molecular Dynamics trajectories. In the first step of the simulated annealing protocol the temperature was increased to 1000 K (500 steps of 10 fs for a total of 5 ps); during this phase the van der Waals radius of the atoms was decreased from 1 to 0.1. In the second step the temperature was slowly lowered to 300 K (1000 steps of 15 fs for a total of 15 ps), and the van der Waals radius was increased from 0.1 to 1. At the beginning of the trajectories, the toxin was positioned randomly at a distance of 15 Å from the channel. All docking trajectories were started with different initial conditions by changing the initial velocities and the initial orientation of the toxin with respect to the channel pore axis. During the simulated annealing the electrostatic energy was turned on toward the end of the dynamics. A continuum solvent model was used with a dielectric constant $\epsilon = 12$ (7). The distance restraint force was fixed to 300 kcal $mol^{-1}Å^{-2}$ during the dynamics.

Flexibility was allowed for the conformation of the toxin backbone of the amino acids 1–3 and of all the toxin side chains. The N terminus backbone of the peptide was allowed to change conformation with respect to the NMR structure following the observation that this region is highly flexible in solution (3). The peptide backbone of residues 4–24 was restrained with an harmonic potential based on the root mean square deviation from the NMR structure with a force of 500 kcal $mol^{-1}Å^{-2}$. This allows rotation and translation of the toxin with respect to the channel while keeping the overall folding close to that experimentally determined. The conformation of the trans-membrane helices of the channel was kept fixed, the backbone of residues 336–386 was restrained to that of the initial model with an harmonic potential and a force of 300 kcal $mol^{-1}Å^{-2}$, whereas the side chains of residues 336–386 were allowed full flexibility.

The MD were followed by 6 cycles of 500 steps of energy minimizations where the backbone restraint function was turned off and the distance restraints were decreased to 75 kcal $mol^{-1}Å^{-2}$. During the minimization the electrostatic potential was turned on.

The trajectories were analyzed using the g_cluster module of the GROMACS 3.1 program (25, 26). The clusters were generated using distances r.m.s.d. with the GROMOS method (27) and a cutoff of 0.2 nm. The r.m.s.d. used to define the clusters is an intermolecular r.m.s.d. containing distances between toxin residues Leu-1, Ser-6, Arg-10, Hyp-13, Hyp-15, Lys-18, and Arg-19 and amino acids Glu-348, Pro-349, Glu-354, Gly-371, and Val-376 of the turret and pore helix region of the four units of the channel.

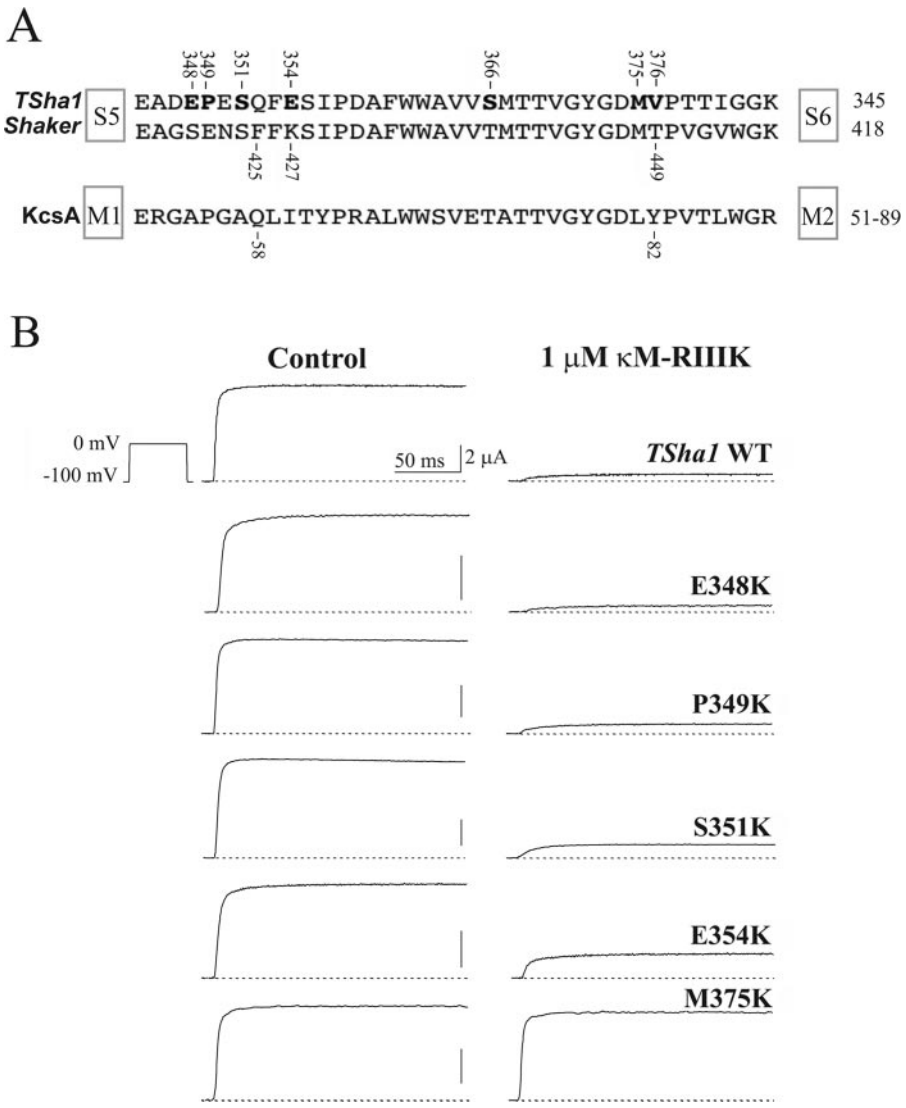

FIG. 1. **Selected site-directed mutations on the pore region of *TSha1* K^+ channels.** *A*, the amino acid alignment of the pore region of the *Shaker* and *TSha1* K^+ channels (S5–S6 linker) and the corresponding region of KcsA bacterial K^+ channel (M1-M2). *B*, whole-cell currents recorded from oocytes expressing *TSha1* mutant channels before and after addition of the κM-RIIIK WT are shown. Notice the apparent slowing of activation of the currents in the presence of toxin illustrating the re-equilibrium of toxin binding to the open state (4). The *dashed lines* correspond to zero current.

RESULTS AND DISCUSSION

We have performed a mutant cycling analysis to identify which amino acids of κM-RIIIK interact with specific residues in the vestibule of the ion channel pore of *TSha1*. For this purpose we have generated several mutants of *TSha1* with single amino acids changes in the pore region of the channel, where κM-RIIIK is likely to interact (4). Fig. 1*A* shows the alignment of the amino acid sequences of the pore region of *TSha1* and *Shaker* together with the one of KcsA, for which a high resolution structure is available (14). Several mutations within this area have been constructed and functionally assayed using the *Xenopus* expression system and two-electrode voltage-clamp experiments. The addition of 1 μM of κM-RIIIK leads to different reductions of the measured currents at a test potential of 0 mV for wild type and mutated ion channels (Fig. 1*B*), demonstrating that the affinity of the peptide for the mutated channels is reduced. For M375K channels, hardly any block can be observed at this toxin concentration. This indicates a very low affinity of the toxin for the mutated channel, which was estimated to be about 10 μM ($k_D \approx 76$ nM for the wild type channel). The changes in the affinity for the different channel mutants are summarized in Table I and confirm that κM-RIIIK indeed interacts with the pore region of the channel. The relative changes induced by the different mutations are summarized in Fig. 2. The mutations E348S, P349K, S351K, M375L, and V376T led to a 2-fold reduction in the affinity of κM-RIIIK. Interestingly the mutation E348K did not have a significant effect despite the drastic change in the electrostatic properties of the side chain. The mutations E354K and E354Q resulted in a decrease of the affinity of 6- and 4-fold, respectively. The mutation M375I resulted in a much stronger affin-

TABLE I
IC_{50} Values for TSha1 mutant K^+ block of κM-RIIIK WT

The IC_{50} values are given by mean values ± S.E. NF, not functional; LE, low expression.

kM-RIIIK	IC_{50} (0 mV)	
	nM	*n*
WT	76 ± 10	9
E348S	110 ± 30	4
E348K	50 ± 10	3
P349K	130 ± 20	3
S351K	160 ± 10	4
E354K	490 ± 110	3
E354Q	270 ± 30	4
S366T	NF	
M375K	10730 ± 2460	3
M375L	140 ± 40	3
M375I	1360 ± 70	5
V376T	120 ± 20	3
V376H	LE	
V376S	NF	
V376E	NF	
V376K	NF	

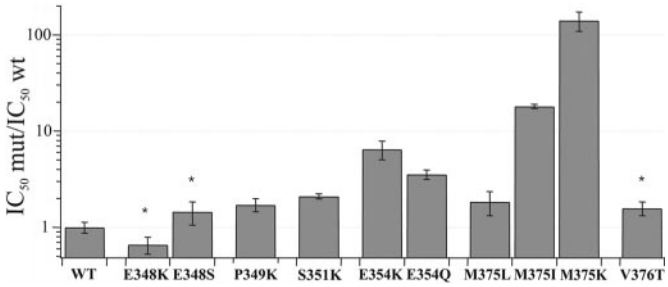

FIG. 2. **Influence of single point mutations in the pore region of *TSha1* on κM-RIIIK binding.** The *bar diagram* shows the affinity of κM-RIIIK to the individual channel mutants normalized to wild type IC_{50}. *Asterisks* represent a non-significant mean value compared with WT (unpaired *t* test).

ity change than M375L (12- *versus* 2-fold), whereas the most dramatic effect was observed for M375K (>100-fold).

To investigate which amino acids of the *TSha1* channel pore interact with specific amino acids of κM-RIIIK, we measured the affinity of several toxin mutants to different ion channel mutants. In this analysis we concentrated on the amino acid residues of the toxin that had been shown to be functionally relevant (Leu-1, Arg-10; Lys-18, Arg-19) (3). The IC_{50} values for the different combinations of channel and toxin mutations are summarized in Table II, whereas Fig. 3 shows the corresponding changes in binding energy ($\Delta\Delta G$) values. Assuming that a $\Delta\Delta G$ value of 2 kJ/mol indicates that the distance between the two mutated residues is less than 6 Å (24), the data of Fig. 3 indicate a quite complex network of interactions between the toxin and amino acids from different domains of the ion channel target.

In our previous work (3) we proposed a new pharmacophore model for the κM-RIIIK-*TSha1* complex based on the fact that the toxin lacks the dyad motif composed of a lysine and a hydrophobic amino acid residue and on the observation that all the functionally relevant residues are clustered on one surface of the peptide delimited by a ring of positive charges. In our model the ring of positive charges is used as an anchor to residues of the K^+ channel loops, and κM-RIIIK blocks the channel by covering the pore as a lid. Additionally, no positively charged side chain penetrates the channel pore. The new pharmacophore is fully supported by the mutant cycling analysis data. Arg-10, Lys-18, and Arg-19 have the largest interactions with residues Glu-348, Pro-349, Ser-351, and Glu-354 of the turret and pore helix regions of the K^+ channel, thus excluding that any of the positively charged side chains penetrates the channel pore. Instead, the positively charged residues interact with the loops of the four channel units, anchoring the peptide to the channel.

The mutant cycling data have been used as intermolecular distance restraints in docking calculations with the aim of obtaining a model for the complex of κM-RIIIK with the *TSha1* channel. The structure of κM-conotoxin RIIIK, determined in aqueous solution by NMR, was docked to the model structure of the *TSha1* channel using the distance restraints derived from the mutant cycle analysis, as described under "Materials and Methods." According to what observed by Eriksson and Roux (7) for the Ag2Tx-*Shaker* complex, we find that one or two distance restraints are insufficient to achieve a selection among the different orientations of the toxin with respect to the channel pore. Therefore, we chose to use all the available distance restraints in the docking calculations. The 875 generated models can be subdivided into 4 clusters, which have been numbered from I to IV according to increasing total energy (Fig. 4). Details on the criterion used for clustering are given under "Materials and Methods." 90% of the generated models belong to cluster I, which also contains the structure with the lowest energy; 6% of the models belong to cluster II, 3% to cluster III, and 1% to cluster IV. No intermolecular distance restraint violations are found in clusters I and II, whereas all structures of clusters III and IV violate the distance restraints Glu-354–Arg-19 and Met-375–Leu-1, respectively. The backbone conformation of the toxin is well defined in all four clusters (toxin backbone r.m.s.d. are 1, 1.4, 1.1, and 1 Å in clusters I, II, III, and IV, respectively). The conformation of the toxin backbone is quite close to the one determined by NMR in cluster I (r.m.s.d. of 1.4 Å), whereas it deviates the most in clusters III (r.m.s.d. of 2.5 Å). The toxin conformations of clusters II and IV have r.m.s.d. values to the NMR-determined conformation of 1.8 and 1.6 Å, respectively. The details of the atomic interactions for the lowest energy structure of each cluster are given in the following section.

The Four Models

Cluster I—The positively charged side chain of Arg-10 of κM-RIIIK is located in a negatively charged pocket of the extracellular loop of unit A of the *TSha1* channel defined by the carbonyls of Pro-349, Glu-350, and Ser-351 and by the side chains of Glu-348, Ser-351, and Glu-354 (Fig. 5). The strong interaction of Arg-10 with Glu-354 accounts for the decreased affinity of κM-RIIIK to the *Shaker* channel, where the homologous position to Glu-354 is occupied by a lysine. The positively charged side chain of Lys-18 is surrounded by the backbone carbonyls of Pro-349, Glu-350, and Ser-351 and the side chains of Glu-348, Ser-351, and Glu-354 of unit C, whereas the Arg-19 interacts with the negatively charged side chain of Glu-354 and with the backbone carbonyl of Ser-351 of unit C (Fig. 5). The electrostatic interactions of Arg-10, Lys-18, and Arg-19 anchor the peptide to the channel loops, stretching it over the channel pore. The interactions of Leu-1 with the channel unit B are both electrostatic and hydrophobic (Fig. 5). The positively charged N terminus is situated among the backbone carbonyl of Glu-348 and the side chains of Gln-352 and Glu-354, justifying the consistent decrease in affinity for the *N*-acetylated toxin (3); the hydrophobic side chain packs against the side chains of Glu-350 and Gln-352 and contacts the methyl groups of Met-375 and Val-376.

Cluster II—The positively charged side chain of Arg-10 contacts the backbone carbonyls of Pro-349, Glu-350, and Ser-351 and the side chains of Glu-348 and Glu-354 of unit A, similarly to cluster I. Lys-18 interacts with the backbone carbonyls of Pro-349, Glu-350, and Ser-351 and with the side chains of Glu-348, Ser-351, and Glu-354 of unit C; Arg-19 contacts the side-chain carbonyls Glu-354 of the same unit C. As for cluster I, the electrostatic interactions of the side chains of Arg-10, Lys-18, and Arg-19 with loop residues of unit A and C stretch the peptide over the channel pore. In cluster II, Leu-1 is situated close to the loop residues of unit D, unlike in cluster I, where Leu-1 contacts the extracellular loop of unit B (Fig. 4). The positively charged N terminal group contacts the side chains of Gln-352 and Glu-354, whereas the Leu side chain has hydrophobic contacts with Pro-349. The distance between the side chain of Leu-1 and the side chains Met-375 and Val-376 in this model is higher than in model I.

Cluster III—As in the clusters I and II, the positively charged side chain of Arg-10 interacts with the backbone carbonyls of Pro-349, Glu-350, and Ser-351 and with the side chain carbonyl of Glu-354 of unit A. The amino group of Lys-18 is situated in a pocket formed by the backbone carbonyls of Pro-349, Glu-350, and Ser-351 and by the side chain of Glu-354 of unit C, whereas Arg-19 contacts the backbone carbonyls of Pro-349 and Glu-350 and the side chain of Glu-354 of unit D. The distance between

TABLE II
IC_{50} values for TSha1 mutant K^+ block of κM-RIIIK WT and analogs

The IC_{50} values (in nM) are given by mean values ± S.E. *n* = number of independent experiments. ND, not done; NB, no block. AcL1, acetyl-Leu-1.

	κM-RIIIK analog IC_{50} values (mean ± S.E.) (*n*)								
	WT	L1A	L1I	AcL1	L1M	R10A	K18A	R19A	K18R/R19K
					nM				
WT	76 ± 10 (9)	3,180 ± 120 (6)	1,380 ± 450 (5)	7,620 ± 380 (5)	340 ± 50 (5)	4,220 ± 330 (7)	3,900 ± 530 (6)	1,530 ± 240 (9)	180 ± 40 (7)
E348S	110 ± 30 (4)	1,920 ± 290 (4)	480 ± 120 (3)	ND	ND	1,220 ± 280 (3)	600 ± 100 (3)	820 ± 210 (4)	100 ± 10 (3)
E348K	50 ± 10 (3)	440 ± 110 (3)	540 ± 100 (4)	ND	ND	770 ± 100 (4)	720 ± 50 (4)	460 ± 60 (4)	150 ± 10 (3)
P349K	130 ± 20 (3)	1,740 ± 110 (3)	280 ± 20 (5)	ND	ND	680 ± 100 (3)	3,390 ± 100 (3)	200 ± 30 (3)	140 ± 10 (4)
S351K	160 ± 10 (4)	2,960 ± 310 (4)	1,700 ± 390 (4)	ND	ND	810 ± 40 (3)	1,390 ± 350 (3)	770 ± 80 (4)	260 ± 60 (3)
E354K	490 ± 110 (3)	14,070 ± 4,740 (3)	1,310 ± 100 (3)	ND	ND	1,640 ± 300 (3)	2,070 ± 220 (3)	740 ± 140 (3)	620 ± 80 (3)
E354Q	270 ± 20 (6)	1,660 ± 80 (5)	1,400 ± 200 (5)	ND	ND	1,700 ± 340 (4)	1,870 ± 350 (4)	1,550 ± 110 (5)	490 ± 30 (4)
M375K	10,730 ± 2,460 (3)	NB	NB	NB	NB	NB	NB	NB	NB
M375I	1,360 ± 70 (5)	11,400 ± 1,030 (3)	4,740 ± 580 (4)	26,610 ± 2,860 (3)	1,360 ± 10 (3)	37,400 ± 7,260 (3)	35,160 ± 7,330 (3)	5,910 ± 790 (4)	1,420 ± 150 (3)
M375L	140 ± 40 (3)	3,260 ± 460 (4)	690 ± 40 (3)	11,400 ± 4,060 (3)	470 ± 50 (3)	ND	ND	ND	ND
V376T	120 ± 20 (3)	3,550 ± 220 (3)	580 ± 180 (3)	ND	ND	2,490 ± 520 (4)	4,650 ± 1,800 (3)	3,990 ± 1070 (3)	310 ± 50 (3)

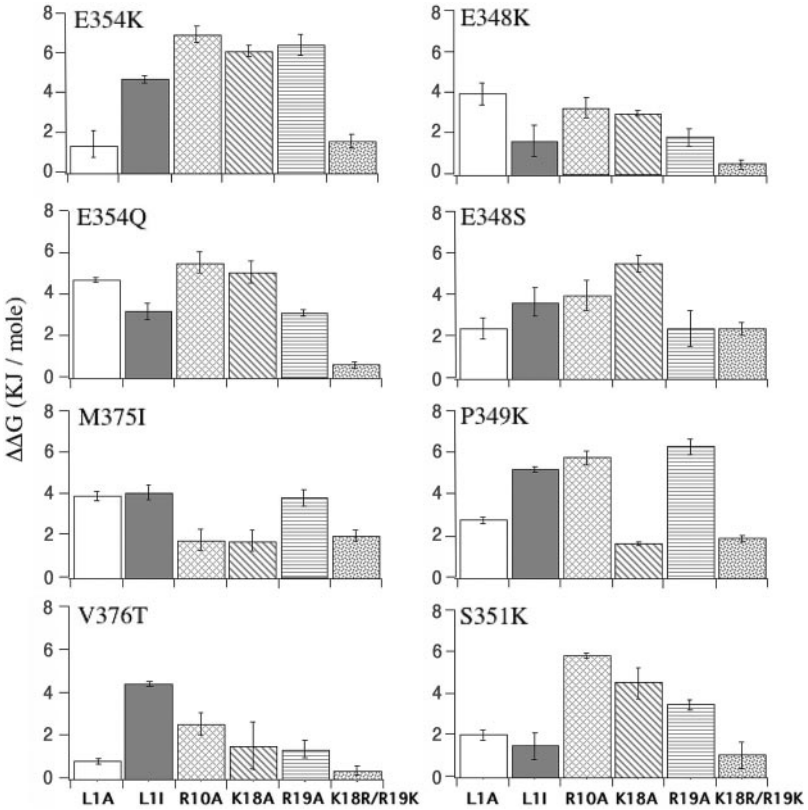

FIG. 3. **Summary of mutant cycle analysis.** Coupling energy (ΔΔ*G* ± S.E.) between *TSha1* mutants and analogs of κM-RIIIK representing important residues for binding (Leu-1, Arg-10, Lys-18, and Arg-19). ΔΔ*G* values exceeding 2.0 kJ/mol indicate coupling interactions within 6 Å distance. L1A mutant (*empty bars*), L1I (*gray-filled bars*), R10A (*net-filled bars*), K18A (*diagonal-stripped bars*), R19A (*horizontal-stripped bars*) and K18R/R19K (*mosaic-filled bars*). All numbers represent the means of 3–6 independent determinations. ΔΔG are taken as absolute values.

the negatively charged side chain of Glu-354 and the positively charged side chain of Arg-19 is larger than in cluster I and II. The positive charge of the arginine side chain is surrounded by several backbone carbonyls and a serine side chain of the toxin itself. Leu-1 is situated close to the extracellular loop of unit D. The positively charged N terminus weakly interacts with the backbone carbonyl of Glu-354; the hydrophobic leucine side chain packs against Pro-349 and Ser-351, whereas the distance to Met-375 and Val-376 is larger than in cluster I.

Cluster IV—The backbone carbonyls of Pro-349 and Glu-350 and the side chain of Glu-354 of unit A interact with Arg-10 as in all other models. The side chains of Glu-348, Gln-352, and Glu-354 of unit C surround Lys-18, whereas Arg-19 stretches over toward the backbone carbonyls of Glu-348 and Pro-349 and the side chains of Glu-348 and Glu-354 of unit D. The positively charged N terminus of Leu-1 interacts with the side chain of Glu-354 of unit D, whereas the Leu side chain only contacts the side chain of Gln-352 and is further from Met-375 than in any other cluster.

In all four clusters the positively charged side chain of Arg-10 is situated in a negatively charged pocket of unit A, defined by the backbone carbonyl of the stretch 348–351 and by the side chain carbonyls of Glu-348 and Glu-354. This reflects the high ΔΔ*G* values observed upon introduction of a positive charge in position 349, 351, and 354 and explains the higher affinity of the toxin for the *TSha1* channel as opposed to the *Shaker* channel, where a lysine is found in the homologous position to Glu-354. The atomic interactions of Lys-18 with loop residues 348–354 are very similar to those of Arg-10. Thus, the two positively charged side chains of Arg-10 and Lys-18 serve as anchors to very similar negatively charged pockets of the channel extracellular loops and pore helix. An additional anchor is represented by Arg-19 that tightly interacts with the side chain of Glu-354. However, Arg-19 can interact either with the same unit as Lys-18 (unit C), as in clusters I and II, or with the neighboring unit, as in clusters III and IV, depending on the conformation of the Arg-19 side chain. This heterogeneity is observed also for structures belonging to the same cluster (1% of the structures of cluster I and 20% of the structures of cluster II). The mutant cycling data and consequently the docking models show that Arg-19 is in closer prox-

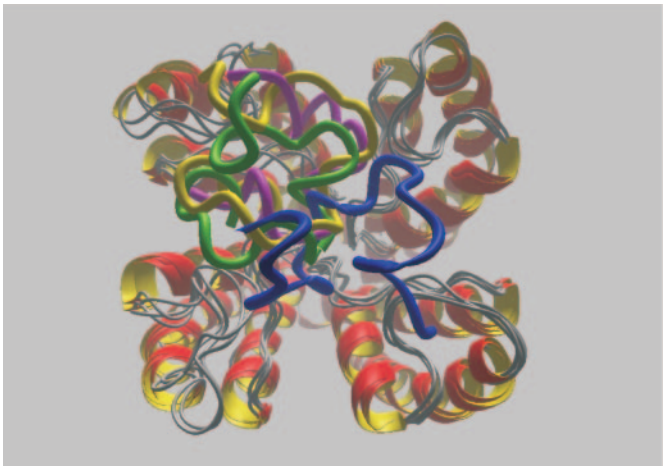

FIG. 4. **The four models for the complex κM-conotoxin RIIIK-*TSha1* K^+ channel.** The backbone of the toxin is represented in *blue* (cluster I), *green* (cluster II), *yellow* (cluster III), and *magenta* (cluster IV). The toxin deeply interacts with only three units of the channel. In cluster I, units A, B, and C are involved in electrostatic and hydrophobic contacts with toxin side chains; in clusters II, III, and IV, units A, C, and D contact the toxin side chains.

imity to the side chain of Pro-349 than Lys-18 ($\Delta\Delta G$ = 6.31 kJ mol^{-1} for the R19A/P349K mutation and 1.67 kJ mol^{-1} for the K18A/P349K mutation).

More complex are the interactions of Leu-1. Mutant cycling data point to the existence of contacts between Leu-1 and Glu-348, Pro-349, Glu-354, Met-375, and Val-376. The distance restraints with Pro-349 and Glu-354 are classified as medium and are reflected in electrostatic contacts of the positively charged N terminus of Leu-1 with the side chain carbonyl of Glu-354. The hydrophobic contacts of Leu-1 are different in the four models; the weak distance restraints with Met-375 and Val-376 are best satisfied in clusters I and II, where Leu-1 reaches Met-375 and Val-376 the closest.

Overall Orientation of the Toxin with Respect to the Channel

Given its small size, κM-RIIIK cannot interact with the extracellular loops of all four units. In all four clusters the toxin contacts three of four units of the K^+ channel. In model I, units A, B, and C bind the toxin, whereas in models II, III, and IV units A, C, and D are involved in contacts with the peptide (Fig. 4). According to the NMR studies (3), the toxin has a discoid shape; in model I the flat surface of the disc is out of the plane defined by the four channel loops, whereas in models II, III, and IV the toxin is flattened on the channel like a pancake. Although the toxin contacts only three of the four units, the accessibility for a potassium ion to the selectivity filter of the channel is reduced by more than 85% in all models.

Does One of the Four Models Better Fit the Mutational Data?

To discriminate between the four models, we analyzed the location of the functionally relevant residues of the toxin with respect to the channel pore (Fig. 6). In our previously published mutational analysis (3), we identified Leu-1, Arg-10, Lys-18, and Arg-19 as being fundamental for binding to the K^+ channel (*red* in Fig. 6); Ser-3, Asn-8, Leu-11, Hyp-13, Val-14, Hyp-15, and Asn-20 resulted to be of medium importance (*yellow* in Fig. 6), whereas mutations of Hyp-2, Ser-6, Leu-7, Leu-9, Hyp-21, and Thr-24 to alanine did not significantly reduce the activity of the toxin (*gray* in Fig. 6). Model I is in very good accord with the mutational data (Fig. 6*A*). All the functionally relevant residues with the exception of Asn-8 face the channel pore or are in contact with the loops, whereas no residue that resulted in being unessential for function strongly interacts with the channel. The only *gray* residue facing the channel pore is Ala-16, for which no mutational data are available. Model II fits the mutational data worse than model I. Three residues of medium importance for binding (Ser-3, Asn-8, and Leu-11) are not in contact with the channel, whereas the C terminus of the toxin, whose side chain was found to be irrelevant for binding, contacts the loop of unit C (Fig. 6*B*). In model III the residues 21–24 at the C terminus of the toxin are involved in several contacts with units C and D, whereas the stretch 11–15, which contains several residues of medium importance for function, points toward solution (Fig. 6*C*). In model IV, the C terminus of the toxin deeply penetrates the channel, and a great portion of the residues that are unimportant for binding interacts with the protein (Fig. 6*D*).

The fact that a whole stretch of functionally relevant toxin residues (residues 11–15) is not in contact with the channel in model III, and IV cannot be taken as the sole argument to exclude these models, as mutations at this site might destabilize the overall structure of the toxin. However, it is rather improbable that amino acids profoundly interacting with the protein (stretch 21–24) can be mutated to alanine without influencing affinity. All in all the mutational analysis data are severely contradicted by models III and IV, allowing us to exclude them as valid representations of the complex between κM-RIIIK and the *TSha1* channel. Model II is retained at this stage, as it does not contradict the mutational data as extensively as model III and IV.

Interaction of κM-RIIIK with the TSha1 Pore

To further discriminate between cluster I and II, we analyzed which part of the toxin is in close proximity to the selectivity filter. For different toxins that interact with voltage-gated K^+ channels there is evidence that a positively charged side chain occludes the channel pore (6–8). This positively charged amino acid is part of the functional dyad together with an amino acid containing a hydrophobic side chain, usually a tyrosine. In our previous work we demonstrated that κM-conotoxin RIIIK does not possess a functional dyad. Moreover, as a result of the mutant cycling analysis, all positively charged amino acids interact with the turret or pore helix regions of the channel and, therefore, cannot penetrate the channel pore. Which toxin residues then face the channel pore in our models? In model I the Hyp-15 is very close to the selectivity filter of units C and B, and the hydroxyl oxygen at the Cγ is at a hydrogen bond distance (2.8 Å) from the carbonyl of the Gly-373 of the selectivity filter of unit B (Fig. 7*A*). In model II the Hyp-13 is in proximity of the selectivity filters of unit A and D but makes no tight direct contact with them (Fig. 7*B*). To distinguish between the two models, mutant cycle data involving the residues of the GYG selectivity filter would be required. This is unfortunately not feasible as any mutation of residues in the selectivity filter destroys the channel activity. Nevertheless, model I and model II can be distinguished by considering the distance of Hyp-13 or Hyp-15 from the amino acid Val-376 of the *TSha1* channel. In model I Hyp-15 is expected to be closer to Val-376 (of unit C) than Hyp-13, while in model II both Hyp-13 and Hyp-15 are at a similar distance from Val-376 of units D and C, respectively. The mutant cycle analysis performed using *TSha1* V376T resulted in a $\Delta\Delta G$ of 0.6 kJ mol^{-1} for O13A and of 2.51 kJ mol^{-1} for O15A, which reflects the geometry of model I much better than that of model II. To obtain further evidence for the interaction of Hyp-15 with the amino acids of the selectivity filter, we assayed the affinity of the O15R and O15K mutants, following the idea that a positive charge should be well tolerated but the bulky arginine should

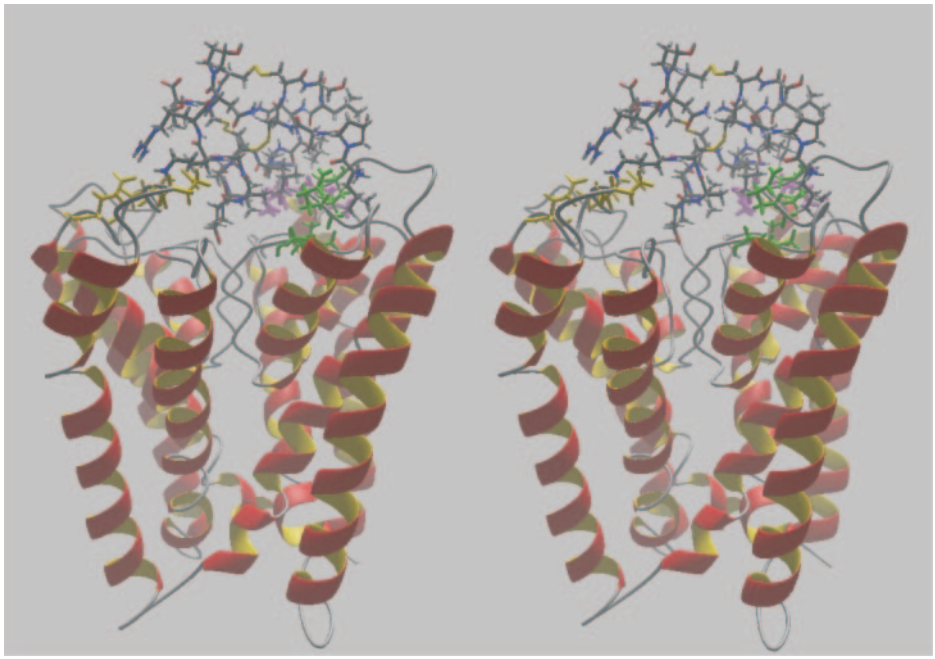

FIG. 5. **Stereo picture of model I showing the details of the electrostatic and hydrophobic interactions of the toxin with the channel.** The amino acids Glu-348, Ser-351, and Glu-354 of unit A (in *magenta*) are in deep contact with the amino acid Arg-10 of the toxin; the same amino acids Glu-348, Ser-351, and Glu-354 of unit C (in *yellow*) contact the side chains Lys-18 and Arg-19 of the toxin, whereas amino acids Glu-350, Gln-352, Met-375, and Val-376 of unit B (in *green*) interact with the charged N terminus and with the hydrophobic side chain of the toxin Leu-1.

not be easily accommodated in proximity of the tight channel pore. The affinity of the mutant O15K for the wild type *TSha1* channel was found to be 430 ± 20 nM (n = 4) against a value of 930 ± 160 nM (n = 3) for the mutant O15A. This indicates that a positive charge in position 15 is preferred to the absence of any polar group, as would be expected if the side chain of Hyp-15 interacts with the carbonyls of the selectivity filter. On the other hand O15R binds the channel with a k_D of 2940 ± 540 nM (n = 4), suggesting that Hyp-15 is situated close to the channel pore, where there is no space to accommodate the bulky arginine side chain. Although these data do not prove directly the interaction of Hyp-15 with residues of the selectivity filter, they strongly support it.

The Best Model

Model I provides a novel pharmacophore for the interaction of toxin peptides with K^+ channels that best explains the mutational and mutant cycle data for the κM-RIIIK-*TSha1* complex. The peptide is anchored to the extracellular loops of three of the four channel units via a basic ring provided by the side chain of Arg-10, Lys-18, Arg-19, and the protonated N terminus of Leu-1, and no positively charged residue occludes the channel pore.

Unlike several other peptides that target voltage-activated K^+ channels, including charybdotoxin from a scorpion, BgK from a sea anemone, and dendrotoxin from snakes, κM-conotoxin RIIIK does not contain a functional dyad of a hydrophobic and a positively charged side chain, which was proposed to be the minimal functional core for K^+ channel-blocking peptides (9–12). The dyad model has been recently challenged by Mouhat *et al.* (13), who demonstrated by mutational analysis and docking calculations that a functional dyad is not strictly required for binding of the scorpion toxin Pi1 to the voltage-gated Kv1.2 potassium channel. Instead, a basic ring of four positively charged side chains was proposed to be a fundamental recognition element by the residue Asp-355 of each of the four Kv1.2 α-subunits. Similarly, we find that four positively charged residues of κM-conotoxin RIIIK are involved in electrostatic interactions with loop and pore helix amino acids of three subunits of the *TSha1* channel. Residue Glu-354 of different units is involved in contacts with all four positively charged residues of the peptide. This amino acid distinguishes the *TSha1* channel, which is the highest affinity target of κM-RIIIK (IC_{50} = 76 ± 10 nM), from other channels of the same family, as for example the *Shaker* (IC_{50} = 1.2 μM) (4), where the homologous position is occupied by a lysine (Lys-427), and Kv1.2 (IC_{50} = 400 nM) (5), where the homologous position is occupied by a neutral proline (Pro-359). Our model suggests that Glu-354 is a fundamental recognition element for κM-RIIIK binding to the *TSha1* channel. However, the complete lack of affinity for κM-RIIIK shown by other members of the Kv1 family (5), which like Kv1.2 contain an uncharged amino acid at position 359, indicates that channel amino acids other than Pro-359 play a comparably important role in toxin recognition. For the toxin it is reasonable to hypothesize that the spatial distribution of the positive charges of the basic ring exerts a fundamental role in channel recognition and provides a solid framework for the high selectivity of the K^+ channel-blocking toxins among the diverse targets.

As shown in the NMR-derived solution structure of the peptide (3), the basic ring defined by Leu-1, Arg-10, Lys-18, and Arg-19 separates the peptide in two faces; all functionally relevant residues, identified by systematic alanine mutations, cluster on one face, which is in contact with the channel in model I.

The mutant cycle analysis excludes that one of the positively charged side chains of κM-RIIIK penetrates the channel pore, as they all interact with amino acids of the extracellular loop and pore helix. In model I the Cγ-hydroxyl of Hyp-15 tightly interacts with the carbonyl of Gly-373 of the unit C selectivity filter. It has been proposed that the carbonyls of the selectivity filter exert an essential role in the coordination of K^+ ions at the entrance of the channel pore (14). Dehydration of the ions must occur at the selectivity filter, as a hydrated K^+ is too large to enter the channel pore. By acting as electron donors, the carbonyls of the selectivity filter replace the water molecules usually associated with K^+ ions in solution, thus compensating for the large energetic penalty of the dehydration process. A H-bond between the Cγ-hydroxyl of Hyp-15 would block one of the selectivity filter carbonyls, seriously disturbing the energetic of the K^+ dehydration process.

A thorough analysis of the binding mode of various scorpion toxins to diverse K^+ channels (28, 29) revealed three possible binding modes that involve different faces of structurally sim-

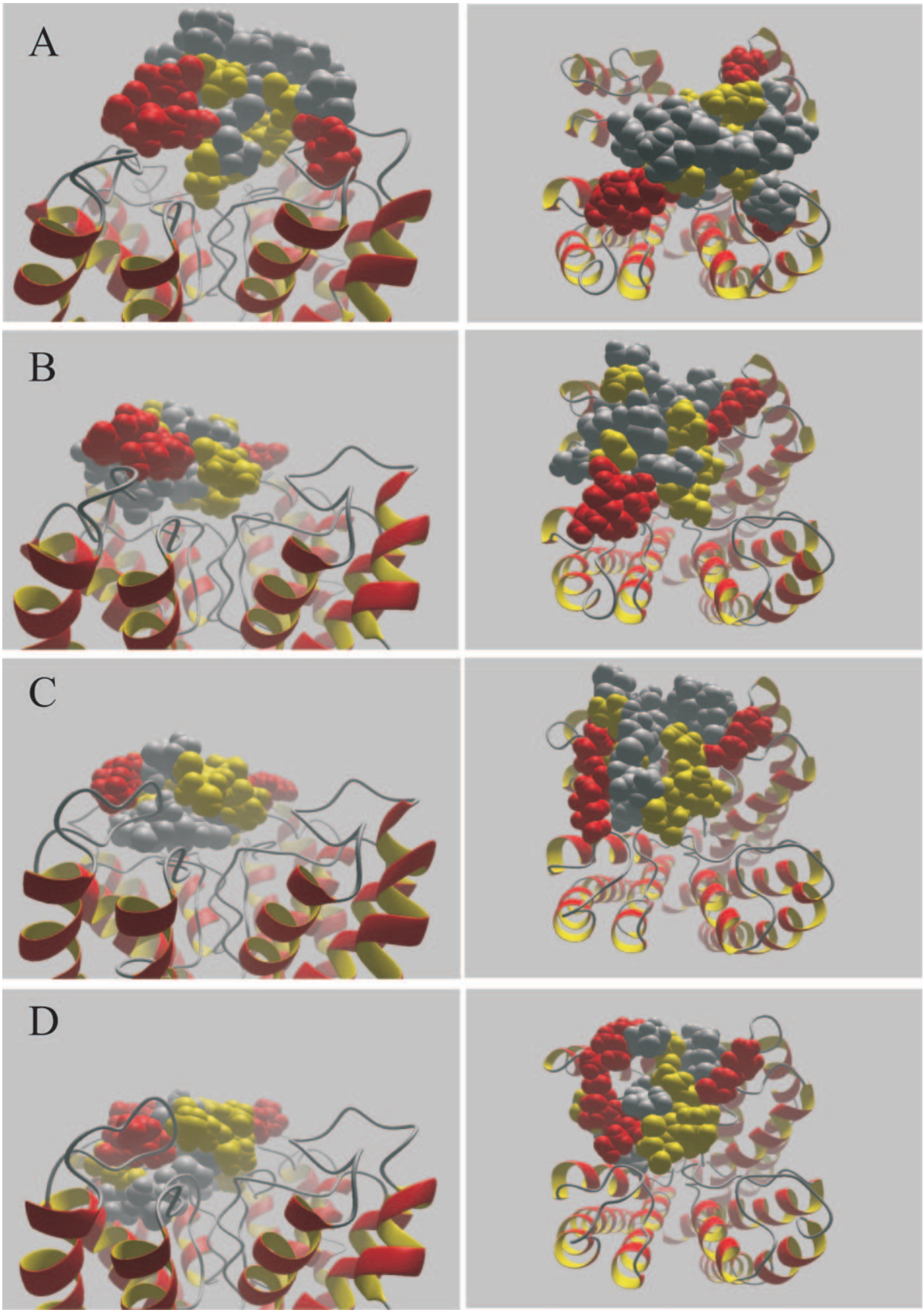

FIG. 6. **Filling space representation of κM-conotoxin RIIIK in the four clusters (clusters I-IV in *panels A–D*), showing the mutational data obtained by systematic alanine substitution (3) in color code.** The functionally most relevant residues are represented in *red* (Leu-1, Arg-10, Lys-18 and Arg-19); the residues of medium importance for binding (Ser-3, Asn-8, Leu-11, Hyp-13, Val-14, Hyp-15, and Asn-20) are shown in *yellow*, whereas the residues that are irrelevant for binding (Hyp-2, Ser-6, Leu-7, Leu-9, Hyp-21, and Thr-24) are in *gray*. Two orientations are provided for each of the four models, from the side (*left panel*) and from the top (*right panel*) of the channel.

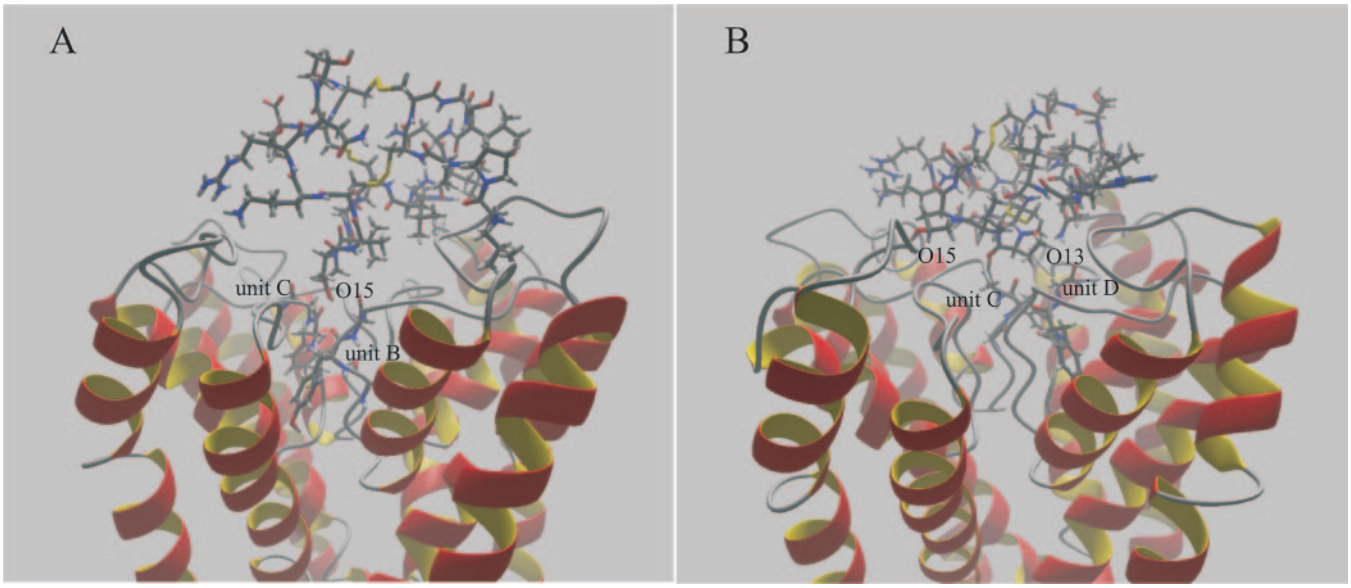

FIG. 7. **Interactions of the residues Hyp-13 and Hyp-15 of κM-conotoxin RIIIK with the selectivity filter of the channel.** In the two *panels A* and *B* models I and II are shown, respectively. The two representations differ for a rotation of about 180° around the channel axis to allow for a better visualization of Hyp-15 in the two models. *A*, model I, the Cγ-OH group of Hyp-15 is close to the selectivity filter of unit B and C and in H-bond distance from the carbonyl oxygen of Gly-373 of unit C. *B*, model II, both Hyp-13 and O15 are close (<5 Å) to the selectivity filter of unit C and D, but no specific interaction can be identified.

ilar toxins; they are the internal binding mode, where residues of the turret region, pore helix, and selectivity filter of the channel are involved, the intermediate mode, involving residues of the turret region, and the external mode, which involves residues far away from the selectivity filter. In the intermediate and external binding mode no functional dyad is observed on the peptide site. This analysis, triggered by the observation that the scorpion toxin BmTx3 can block both A-type K^+ and HERG currents (30) using different functional faces, confirms the existence of different binding modes of peptidic toxins to K^+ channels, some of which do not involve a direct obstruction of the pore by a positively charged side chain. Based on the solution structure and the mutational analysis of κM-RIIIK, we proposed that this toxin could bind the *TSha1* channel in the intermediate mode. However, the mutant cycle data and the docking model I prove the interaction of toxin residues with amino acids in the turret and pore helix regions and to some extent also with the selectivity filter. In the classification of Rodriguez de la Vega *et al.* (28), the position of the toxin in the κM-RIIIK-*TSha1* channel complex resembles the internal binding mode best. However, the side chain of Hyp-15 does not completely occlude the channel pore as the lysine of the functional dyad but rather disturbs the charge distribution at the selectivity filter by involving one of the carbonyls in a H-bond.

Despite the entirely different pharmacological specificity and many differences in the amino acid sequence, κM-conotoxin RIIIK shows striking structural similarities to μ-conotoxin GIIIA (31–33), which specifically blocks NaV1.4 Na^+ channels. κM-conotoxin RIIIK and μ-conotoxin GIIIA belong to the same phylogenetic family and share a common pattern of cysteine bridges. Interestingly, Hyp-15 of κM-conotoxin RIIIK is at the homologous position of Arg-13, the Na^+ channel pore occluding residue in the peptide sequence of μ-conotoxin GIIIA. This fact together with the high structural similarity of the two toxins suggests that κM-conotoxin RIIIK and μ-conotoxin GIIIA might block K^+ and Na^+ channels, respectively, with a similar geometry. However, because the O15R mutant of κM-RIIIK is inactive on $Na_v1.4$ sodium channels (data not shown), additional parameters must be involved in determining the selectivity of the two peptides for Na^+ or K^+ channels. Similarly to κM-RIIIK, a ring of positively charged side chains can be identified on μ-GIIIA as well (3). Most likely the overall shape of the two peptides and the charge distribution of the basic ring are key determinants for the Na^+ or K^+ channel selectivity of μ-conotoxin GIIIA and κM-conotoxin RIIIK.

Conclusions

We have presented a combined approach based on thermodynamic mutant cycle data and docking calculations to derive the structure of the complex of κM-conotoxin RIIIK with the K^+ channel *TSha1*. This peptide shows a novel binding mode to the K^+ channel that is not centered around a functional dyad. Instead, a ring of positive charges anchors the peptide to the turret and pore helix region of the channel; the electrostatic complementarity between this ring and the channel side chains is likely to be responsible for the selectivity of κM-RIIIK toward the *TSha1* channel, as it can be inferred from the important role of Glu-354 of different units in contacting the basic ring. This amino acid is not present in lower affinity targets of κM-RIIIK, such as the *Shaker* channel. The intermolecular interactions involving the channel loops and the toxin positively charged side chains can be of general importance in determining the selectivity of peptidic toxins for ion channels.

The role of the positive charged side chain that in many peptide-ion channel complexes occludes the channel pore is partially exerted by Hyp-15, whose side chain, however, is too short to penetrate the pore. The Cγ-OH of Hyp-15 contacts the carbonyls of the selectivity filter of one to two units, perturbing the electrostatic forces that regulate the dehydration of potassium ions at the pore entrance.

The binding mode of κM-RIIIK to the *TSha1* channel closely resembles that of μ-conotoxin GIIIA to the $Na_v1.4$ Na^+ channel. The three-dimensional structure of the two peptides is highly similar in the C-terminal part despite the poor superposition of the amino acid sequence. Hyp-15 of κM-RIIIK occupies the homologous position of Arg-13 of μ-GIIIA, which is known to occlude the Na^+ channel pore. Both peptides contain a basic ring, although the form and the charge density at the surface differs (3). This observation demonstrates that the two

conotoxins have developed a similar scaffold and binding geometry to their respective targets, whereas the pharmacological selectivity is determined by the exact charge distribution and three-dimensional shape.

REFERENCES

1. Hille, B. (2001) *Ion Channels of Excitable Membranes*, 3rd Ed., Sinauer Associates, Inc.
2. Terlau, H., and Olivera., B. M. (2004) *Physiol. Rev.* **84,** 41–86
3. Al-Sabi, A., Lennartz, D., Ferber, M., Gulyas, J., Rivier, J. E. F., Olivera, B. M., Carlomagno, T., and Terlau, H. (2004) *Biochemistry* **43,** 8625–8635
4. Ferber, M., Sporning, A., Jeserich, G., DelaCruz, R., Watkins, M., Olivera B. M., and Terlau H. (2003) *J. Biol. Chem.* **278,** 2177–2183
5. Ferber, M., Al-Sabi, A., Stocker, M., Olivera, B. M., and Terlau, H. (2004) *Toxicon* **43,** 915–921
6. Miller, C. (1995) *Neuron* **15,** 5–10
7. Eriksson, M. A. L., and Roux, B. (2002) *Biophys. J.* **83,** 2595–2609
8. Gao, Y.-D., and Garcia, M. (2003) *Proteins* **52,** 146–154
9. Dauplais, M., Lecoq, A., Song, J., Cotton, J., Jamin, N., Gilquin, B., Roumest C., Vita, C., de Medeiros, C. L. C., Rowan E., Harvey, A. L., and Ménez, A. (1997) *J. Biol. Chem.* **272,** 4802–4809
10. Savarin, P., Guenneugues, M., Gilquin, B., Lamthanh, H., Gasparini, S., Zinn-Justin, S., and Ménez, A. (1998) *Biochemistry* **37,** 5407–5416
11. Gilquin, B., Racape, J., Wrisch, A., Visan, V., Leqog, A., Grissmer, S., Menez A., and Gasparini, S. (2002) *J. Biol. Chem.* **277,** 37406–37413
12. Srinivasan, K. N., Sivaraja, V., Huys, I., Sasaki, T., Cheng, B., Kumar, T. K. S., Sato, K., Tytgat, J., Yu, C., Ching San B. C., and Ranganathan, S., Bowie, J. H., Kini, R. M., and Gopalakrishnakone, P. (2002) *J. Biol. Chem.* **277,** 30040–30047
13. Mouhat, S., Mosbah, A., Visan, V., Wulff, H., Delpierre, M., Darbon, H., Grissmer, S., De Waard, M., and Sabatier, J.-M. (2004) *Biochem. J.* **377,** 25–36
14. Doyle, D. A., Cabral, J. M., Pfuetzner, R. A. Kuo, A. L., Gulbis, J. M., Cohen, S. L., Chait B. T., and MacKinnon R. (1998) *Science* **280,** 69–77
15. Hidalgo, P., and MacKinnon, R. (1995) *Science* **268,** 307–310
16. Sato K., Ishida, Y. Wakamatsu, K. Kato, R. Honda, H. Ohizumi, Y. Nakamura, H. Ohya, M. Lancelin, M. Kohda D., and Inagaki, F. (1991) *J. Biol. Chem.* **266,** 16989–16991
17. Becker, S., Prusak-Sochaczewski, E., Zamponi, G., Beck-Sickinger, A. G., Gordon, R. D., and French, R. J. (1992) *Biochemistry* **31,** 8229–8238
18. Ishii, T. M., Zerr, P., Xia, X. M., Bond, C. T., Maylie, J., and Adelman, J. P. (1998) *Methods Enzymol.* **293,** 53–71
19. Sambrook, J., and Russell, D. W. (2001) *Molecular Cloning: A Laboratory Manual*, 3rd Ed., Cold Spring Harbor Laboratory Press, Cold Spring Harbor, NY
20. Jacobsen, R. B., Koch, E. D., Lange-Malecki, B., Stocker, M., Verhey, J. F., Van Wagoner, R. M., Vyazovkina, A., Olivera, B. M., and Terlau, H. (2000) *J. Biol. Chem.* **275,** 24639–24644
21. Sali, A., and Blundell, T. L. (1993) *J. Mol. Biol.* **234,** 779–815
22. Brünger, A. T., Adams, P. D., Clore, G. M., DeLano, W. L., Gros, P., Grosse-Kunstleve, R. W., Jiang, J.-S., Kuszewski, J., Nilges, M., Pannu, N. S. Read, R. J., Rice, L. M., Simonson, T., and Warren, G. L. (1998) *Acta Crystallogr. Sect. D* **54,** 905–951
23. Ranganathan, R., Lewis, J. H., and MacKinnon, R. (1996) *Neuron* **16,** 131–139
24. Schreiber, G., and Fersht, A. R. (1995) *J. Mol. Biol.* **248,** 478–486
25. Berendsen, H. J. C., van der Spoel, D., and van Drunen, R. (1995) *Comput. Phys. Commun.* **91,** 43–56
26. Lindahl, E., Hess, B., and van der Spoel, D. (2001) *J. Mol. Model* **7,** 306–317
27. Daura, X., Gademann, K., Jaun, B., Seebach, D., van Gunsteren W. F., and Mark A. E. (1999) *Angew. Chem. Int. Ed.* **38,** 236–240
28. Rodriguez de la Vega, R. C., Merino, E., Becerril, B., and Possano, L. D. (2003) *Trends Pharmacol. Sci.* **24,** 222–227
29. Xu, C.-Q., Zhu, S.-Y., Chi, C.-W., and Tytgat, J. (2003) *Trends Pharmacol. Sci.* **24,** 446–448
30. Huys, I., Xu, C.-Q., Wang, C.-Z., Vacher, H., Martin-Eauclaire, M.-F., Chi, C.-W., and Tytgat, J. (2004) *Biochem. J.* **378,** 745–752
31. Hill, J. M., Alewood, P. F., and Craik, D. J. (1996) *Biochemistry* **35,** 8824–8835
32. Lancelin, J. M., Kohda, D., Tate, S., Yanagawa, Y., Abe, T., Satake, M., and Inagaki, F. (1991) *Biochemistry* **30,** 6908–6916
33. Wakamatsu, K., Kohda, D., Hatanaka, H., Lancelin, J. M., Ishida, Y., Oya, M., Nakamura, H., Inagaki F., and Sato, K. (1992) *Biochemistry* **31,** 12577–12584